IEEE Access
Multidisciplinary | Rapid Review | Open Access Journal

Date of submission 15 Feb. 2022

Digital Object Identifier ...

Sub-6 GHz and mm-Wave 5G Vehicle-to-Everything (5G-V2X) MIMO Antenna Array

MUHAMMAD IKRAM[1], (Member, IEEE), KAMEL SULTAN[1], (Student Member, IEEE), AMIN ABBOSH[1],(Fellow, IEEE), and NGHIA NGUYEN-TRONG[2], (Member, IEEE)

[1]School of Information Technology and Electrical Engineering, The University of Queensland (UQ), Brisbane, 4072 Australia.
[2]School of Electrical and Electronic Engineering, The University of Adelaide, Australia.

Corresponding author: Muhammad Ikram (e-mail: m.ikram@uq.edu.au & ikram439@gmail.com).

ABSTRACT A multi-beam and multi-polarized Multiple-Input Multiple-Output (MIMO) antenna system, which operates at Sub-6 GHz and mm-wave frequency bands is realized for 5G Vehicle-to-Everything (5G-V2X) application. Since the vehicle needs to communicate in different scenarios with the others, e.g. vehicles, passengers, control units, and mobile networks, in the surrounding area, an antenna with 360° coverage area is required. In this paper, an eight-element MIMO antenna is designed and implemented for this purpose. Four elements are distributed evenly in a circular substrate placed in the azimuth plane. Meanwhile, the other four elements are printed on two orthogonal substrates which are fixed perpendicularly to the circular substrate. Each radiating component is a tapered slot antenna integrated with a dipole to operate at both microwave and mm-wave bands. The simulated and measured results demonstrate capability of the proposed design in covering the whole surrounding area (360° coverage in azimuth plane). The antenna achieves a realized gain of more than 9 dBi at the mm-wave range and 4 dBi at the microwave range.

INDEX TERMS Dipole antenna, intelligent transportation, microwaves, mm-waves, tapered slot antenna, Vehicle-to-everything (V2X), 5G.

I. INTRODUCTION

RECENTLY, the development of wireless communication technologies has led to parallel development in the concept of intelligent transportation systems (ITS) to improve the safety and security of drivers and pedestrians. Thus, the ITS has been moved forward to include vehicle-to-everything (V2X), which comprises vehicle-to-infrastructure (V2I), vehicle-to-cloud (V2C), vehicle-to-vehicle (V2V), vehicle-to-pedestrian (V2P), and vehicle-to-network (V2N) [1], [2], as illustrated in Fig. 1. With this development direction, the Third Generation Partnership Project (3GPP) community defined the cellular network as the bone platform connection for V2X technology, mentioned as cellular V2X (C-V2X) [2], [3]. Towards an intelligent transportation system, C-V2X plans to reduce road accidents by 80% [3]. Thanks to the massive device connectivity, high data rate, and low service latency, along with the 5G's capability, 5G-V2X will provide high-performance remote driving, map, video sharing vehicle platooning, and collision avoidance system [4]. The benefits of using 5G come from using millimeter-wave (mm-wave) communication to meet the increased traffic demands [3], [5], [6].

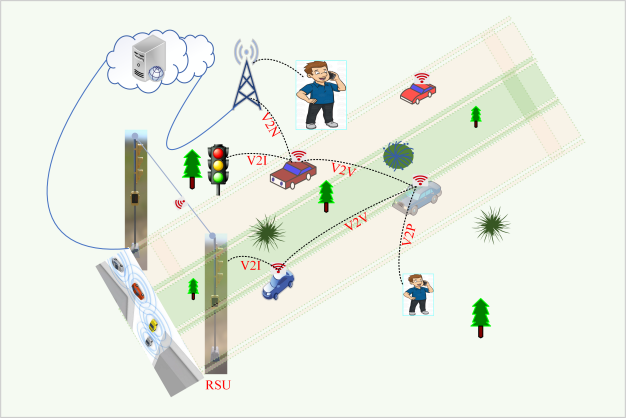

FIGURE 1. The conceptual scenario of 5G-V2X communication services.

Generally, V2X have the following communication scenar-

This article has been accepted for publication in a future issue of this journal, but has not been fully edited. Content may change prior to final publication. Citation information: DOI 10.1109/ACCESS.2022.3172931, IEEE Access

ios to be considered:

1) V2V: allowing the vehicles to communicate directly in close contact. Such a type of connection is short and medium-range communications that can work at a higher frequency to achieve a high data rate. Essentially, it is intended to improve road safety, such as collision avoidance; as a result, high dependability and low latency are required for such V2V connections.
2) V2P: providing the connection between the vehicle and vulnerable road users via mobile network, including medium and long-range communications.
3) V2I: sharing the delay-intensive information with road-side units (RSU). Since the radio range of RSU is short, the data should be shared at a high rate.
4) V2N: providing a connection between the vehicle and remote servers for navigation information, real-life traffic state, and weather conditions.

Since the services of V2X have different requirements in terms of range and data rate, diverse frequency ranges of 5G are required to meet those needs. It is well known that the upcoming 5G network support mm-wave band and sub-6 GHz bands, which serve all the scenarios mentioned above of V2X. Small size, low cost, highly efficient, dual bands (lower and mm-wave band), and 360° area coverage of the road are the main antenna specifications that should be achieved.

While 5G applications are benefited from the wide bandwidth at mm-wave, the propagation in this frequency range faces high attenuation which restricts the link budget. Thus, high gain is needed besides the required wide coverage area for such type of V2X applications [7]–[10]. In recent literature, the antenna arrays, such as sub-arrays, reconfigurable antennas [11], [12], phased arrays, and beam switching antennas [8], [10], [13]–[16] are used as a solution to increase coverage area at mm-wave range. The phased antenna arrays have limitations in terms of bulky or lossy phase shifters, size, high efficiency, and bandwidth. The other solution of using an antenna array with beamforming of feeding network is complicated and lossy, especially for antenna arrays with a large scale. The antennas in [17], [18] are based on the lens antenna to achieve high gain but suffer from complicated multi-layered structures, narrow-bandwidth, and high loss. Furthermore, the designs in [19], [20] with Buttler matrix have high loss and low efficiency resulting from the feeding network. It is noted that the aforementioned solutions still do not provide the required 360^o coverage. Besides, they only cover the upper band of the 5G applications. A multi-polarized antenna based on the combination of loop dipoles and monopole was reported in [4] to serve the 5G-V2X. This antenna covers the 5G sub-6 GHz only with a relatively complicated structure. A slot cavity-backed antenna array, which uses a simple feeding network without power diver to reduce losses and a full metal box to increase gain, is presented in [21] as a candidate of C-V2X around 3GHz. Despite achieving high gain, it has low coverage efficiency and does not support the mm-wave band of 5G. Finally, to support both lower and upper bands of 5G, several studies were introduced in [22]–[28]; however, these antennas have small coverage area due to the limited space implemented in mobile handsets.

In this paper, a tapered slot antenna array with a simplified structure is proposed to meet the requirement of 5G-V2X application. This antenna can simultaneously operate at sub-6 GHz to realize V2P and V2N communication and mm-wave with 360^0 coverage area in azimuth plane to realize V2V and V2I communications. It achieves high gain for the communication on high-way roads. The antenna array consists of eight elements: four arranged on a horizontal circular substrate, whereas the other four are placed on two vertical cross-shaped substrates. This configuration of the design is utilized to increase the coverage area where each antenna covers a region of 45° in azimuth plane. Moreover, the diversity between elements leads to the improvement in the MIMO performance.

II. ANTENNA DESIGN CONCEPT, AND OPTIMIZATION OF SINGLE ELEMENT

A. DESIGN CONCEPT

A conventional tapered slot antenna operates at a single band and provides end-fire radiation patterns [29]. In our proposed design, the tapered slot is used to feed a dipole structure and operates as a wideband end-fire antenna. With the combination of tapered slot and dipole structures, the overall footprint of the single antenna is reduced while providing multi-band characteristics. The combined antenna element covers the sub-6 GHz and mm-wave bands, which is the key feature of the proposed design. Then this antenna element is replicated and arranged in one circular and two crossed-shaped substrates to develop a compact shared-aperture multi-beam and multi-band Multiple-Input Multiple-Output (MIMO) antenna system as shown in Fig. 2. The antenna elements are denoted as Ant. i for $i = 1, 8$.

B. SINGLE ELEMENT ANTENNA GEOMETRY

The design evolution for each antenna element, e.g. Ant. 1, is illustrated in Fig. 3. A Rogers 5880 substrate with dielectric constant of 2.2 and loss tangent of 0.0009 at 10 GHz is used. The design starts with a typical printed dipole antenna fed by a quarter-wavelength slot (Step-1). The structure is designed to operate at 2.6 GHz. The dipole and slot are printed on the bottom side of the substrate. A 50-Ω transmission line, which is printed on the top side of the substrate, is used to excite the structure at 2.6 GHz. The length of dipole (d_L) is adjusted to tune the operating frequency at the desired band as shown in Fig. 4.

A Vivaldi or tapered slot antenna (TSA) can be utilized to generate a directional radiation beam. First, a TSA is designed at the same location as the feeding slot of the dipole antenna as shown in Step 2 of Fig. 3. The TSA can be designed based on the procedure presented in [30], [31] to operate at 28 GHz. The optimized performance of the TSA is shown in Fig. 5. It can be observed that the TSA covers

This article has been accepted for publication in a future issue of this journal, but has not been fully edited. Content may change prior to final publication. Citation information: DOI 10.1109/ACCESS.2022.3172931, IEEE Access

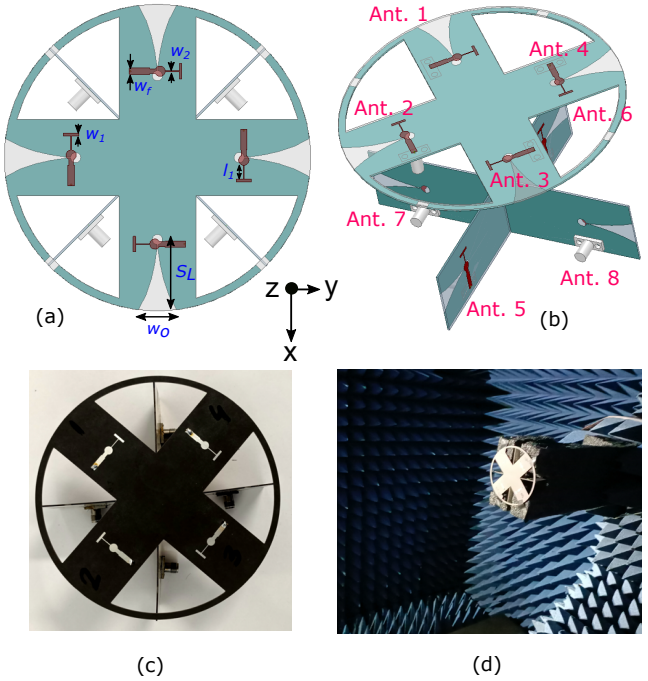

FIGURE 2. The complete MIMO antenna design with critical design parameters. (a) geometry (b) expanded version of the design, (c) fabricated prototype, and (d) measurements inside Anechoic chamber. The optimized dimensions of the parameters in millimetres (mm) are: S_L= 30, w_o= 15, w_f= 2.43, w_1= 1, w_2= 0.3, and l_1= 5.5.

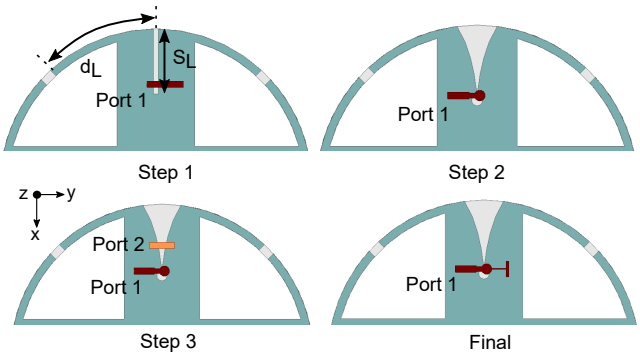

FIGURE 3. Design steps of each antenna element, e.g. Ant. 1 shown in Fig. 2.

the 28-GHz 5G band with a very wide −10-dB impedance matching bandwidth. The 2D realized gain cuts at $\theta = 90°$ (dotted line) and $\phi = 0°$ (solid line) are also presented in Fig. 5 showing directive radiation beams towards endfire directions.

Aiming to achieve a shared-aperture antenna operating at sub-6 GHz and mm-wave bands, the dipole and tapered slot antenna are excited altogether in a hybrid structure as shown in Step 3 of Fig. 3. In this structure, the rectangular slot in the initial dipole structure (Step 1) is replaced by a tapered slot. At this stage, two feeds are used to excite the combined structure. The matching performance for Step 3 is shown Fig. 6 (solid blue curve). It can be observed that the structure with dual-feed provides dual-band performance at sub-6 GHz

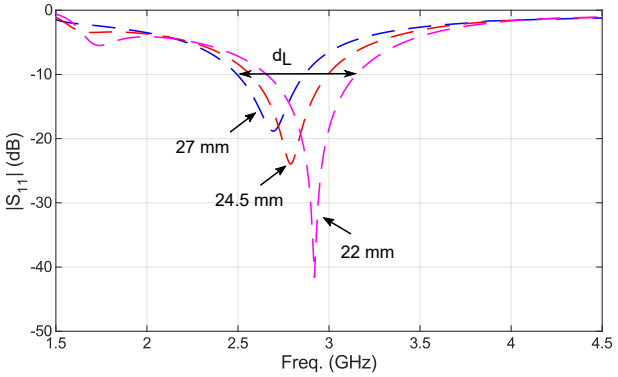

FIGURE 4. Effect of d_L on the dipole resonance (Step 1 in Fig. 3).

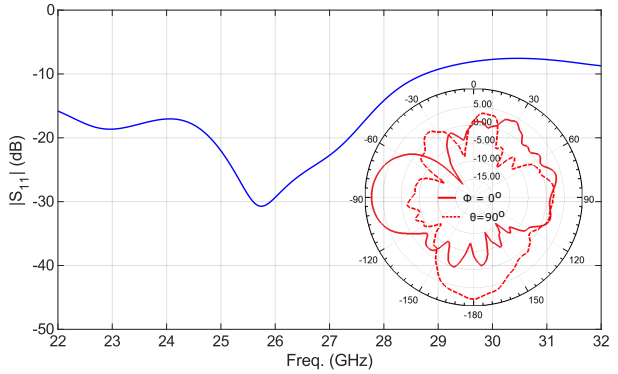

FIGURE 5. Performance of the TSA (Step 2) at 28 GHz.

and 5G mm-wave bands.

All results from Step 1 to Step 3 (Fig. 3) are further verified with the simulated current distributions shown in Fig. 7. In Step 1 (or Step 2), the currents are mostly concentrated along the arms of the dipole (or along the TSA). For Step 3, each radiating element is excited at the corresponding operating frequency.

To make the design simple for verification as a proof of concept, instead of using two feeding ports (Step 3), a single feeding structure is constructed, as illustrated in the Final step of Fig. 3. To match the feed with the dual frequency with such a large frequency ratio, a quarter-wavelength stub is added with the feed designed in Step 3. This stub also acts as a band-stop filter at 28 GHz band [32]. The design in Final step is optimized with the single feeding and a stub to achieve optimal performance in terms of bandwidth and gain. The performance of the final structure (Ant. 1) is shown in Fig. 6. It should also be noted that with the tapered slot configuration, the sub-6 GHz band is much wider compared to the initial structure with the rectangular slot. This is because the dipole and tapered slot resonances combine with each other and ultimately provides wider bandwidth. It covers 2.6 GHz band from 2.4 GHz to 3.5 GHz with −10-dB impedance matching bandwidth. At the same time, it also provides a wideband −10-dB impedance bandwidth at 28-GHz 5G band. The final optimized parameters are listed in

This article has been accepted for publication in a future issue of this journal, but has not been fully edited. Content may change prior to final publication. Citation information: DOI 10.1109/ACCESS.2022.3172931, IEEE Access

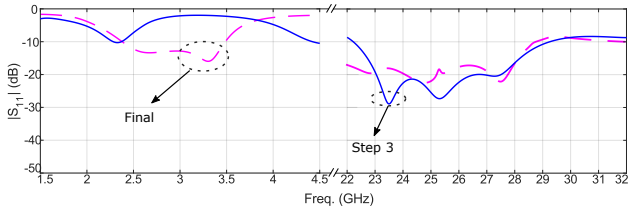

FIGURE 6. Performance of the hybrid tapered slot - dipole at 3 GHz and 28 GHz.

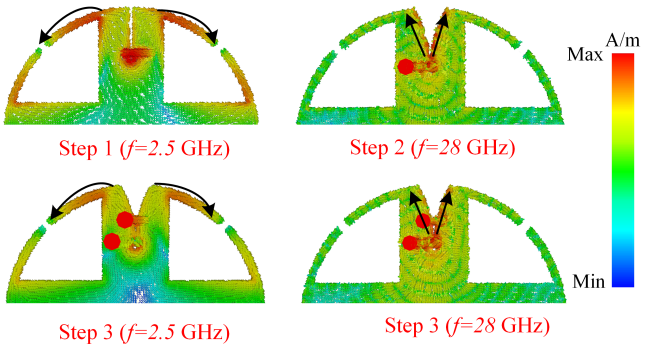

FIGURE 7. Simulated current distributions for different design steps.

the caption of Fig. 2.

III. MIMO CONFIGURATION, OPERATION, AND DISCUSSIONS

This section aims to investigate and develop a multi-beam and multi-band Multiple-Input Multiple-Output (MIMO) antenna system with compact and shared-aperture configuration. The complete MIMO antenna system with fabrication prototype and measurements environment is shown in Fig. 2.

Following the optimization of one antenna element, i.e. Ant. 1, it is replicated and placed around a circular-shaped substrate, which has a diameter of 120 mm and thickness of 0.79 mm, along the x-axis (Ant. 3) and y-axis (Ant. 2 and Ant. 4). This configuration is constructed to produce 4 separate beams (see Fig. 8) with a reasonably high isolation among antenna elements at both sub-6 GHz and mm-wave bands.

To achieve a better coverage in the azimuth plane, two crossed-shaped substrates (height of 30 mm and length of 120 mm) are utilized and placed at $\phi = 45^o$ and $\phi = 135°$ in xy-plane. Then, four antenna elements are placed on the four edges at $\phi = -45°$ (Ant. 5), $\phi = 135°$ (Ant. 6), $\phi = -135°$ (Ant. 7) and $\phi = 45°$ (Ant. 8), of those crossed-shaped substrates as illustrated in Fig. 2. This configuration can provide a full coverage (360°) in xy-plane with relatively high gain, which is especially useful for the 5G-V2X communication.

The performance of the proposed MIMO antenna design is also considered with a circular metallic surface (diameter = 200 mm), e.g. to mimic the roof of a vehicle [33]. This metallic surface is placed underneath the proposed design as shown in Fig. 9. Since the proposed design is based on

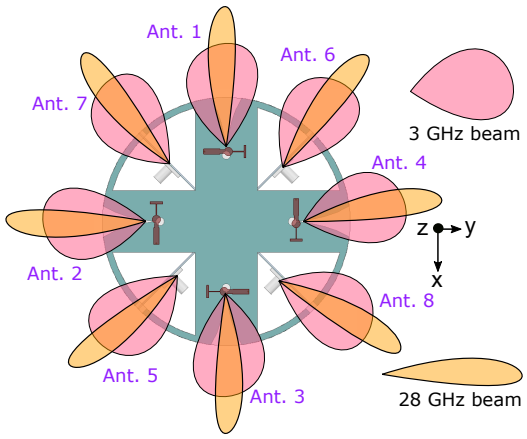

FIGURE 8. The conceptual diagram of radiation patterns for the eight antennas at 3 GHz and 28 GHz bands showing a large spatial coverage.

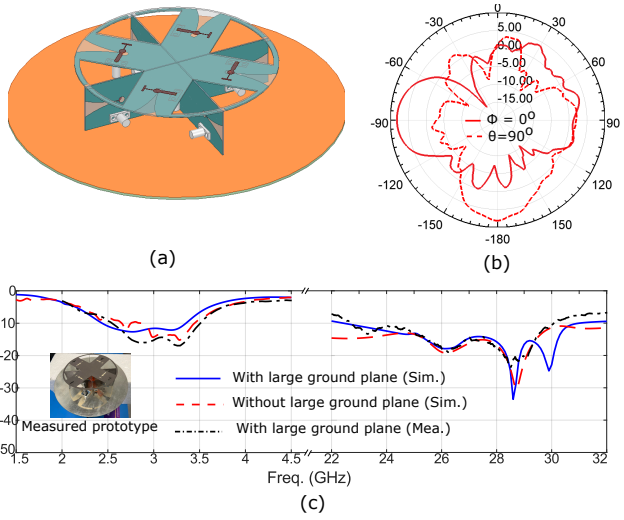

FIGURE 9. The proposed MIMO antenna placed on the metallic surface. (a) simulated structure, (b) 2-D radiation patterns at 28 GHz, and (c) simulated and measured S_{11} at sub-6 GHz and mm-wave bands.

a tapered slot antenna which has directional characteristics, there is no significant change in the performance of the design (the performance of Ant. 1 is shown in Fig. 9 for brevity). Therefore, a proposed MIMO antenna system can be installed directly over the roof of a vehicle.

A. S-PARAMETERS

Due to symmetry of the design, only simulated and measured reflection coefficients for Ant. 1, Ant. 2, Ant. 5, and Ant. 6 are presented in Fig. 10 for brevity. In general, the measured reflection coefficient curves are in line with the full-wave simulations. The discrepancy in the measured and simulated results is attributed to the fabrication and measurement tolerances. It is noted that since the length of the dipole arm in Ants. 5, 6, 7 and 8 is not maintained to be exactly the same as Ant. 1, a slight change in the reflection coefficient is observed in Fig. 10. Nevertheless, all antennas still have

This article has been accepted for publication in a future issue of this journal, but has not been fully edited. Content may change prior to final publication. Citation information: DOI 10.1109/ACCESS.2022.3172931, IEEE Access

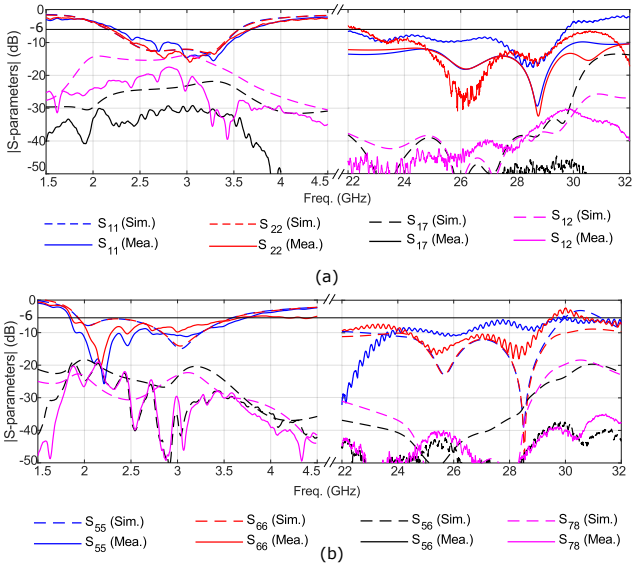

FIGURE 10. Simulated and measured S-parameters for the whole MIMO antenna system.

wide bandwidths at both sub-6 GHz and mm-wave bands with return loss better than 6 dB. The results show that the proposed MIMO design can operate at 2.45, 2.6 and 3.4 GHz (WLAN, LTE, 5G) sub-6 GHz bands with −6-dB impedance bandwidth from 2.30 to 3.5 GHz. It also can be seen that Ant. 1 to Ant. 8 operate at 28 GHz (5G) with −10-dB impedance matching bandwidth from 26 to 29 GHz. The simulated and measured isolation (S_{ij}) among antenna elements is more than 15 dB at both sub-6 GHz and mm-wave bands.

B. RADIATION PATTERNS AND GAIN

The radiation patterns of the proposed MIMO antenna system are measured in an anechoic chamber as shown in Fig. 2. Different simulated and measured 2D cuts are selected to show the direction of the main beams. Figs.11 and 12 depict the simulated and measured normalized radiation patterns for Ant. 1, 2, 3 and 4 at 3 GHz and 28 GHz, respectively. Meanwhile, Figs. 13 and 14 plot the simulated and measured normalized radiation patterns for Ant. 5, 6, 7 and 8 at 3 GHz and 28 GHz, respectively. One immediate observation is that all radiated beams point towards different directions in both bands which is desirable for MIMO communication to reduce channel correlation. Moreover, all antenna elements provide large beamwidth at 3 GHz and small beamwidth at 28 GHz which verify that realized gain at sub-6 GHz bands is less than mm-wave bands. A high gain values are desirable at mm-wave bands to compensate the high path loss at mm-wave bands. The simulated and measured realized gain values are listed in Table I. A maximum measured realized gain of 4.5 dBi and 9.8 dBi is observed at 3.4 GHz and 28 GHz, respectively. A good agreement between simulated and measured results is obtained for both radiation patterns and gain values.

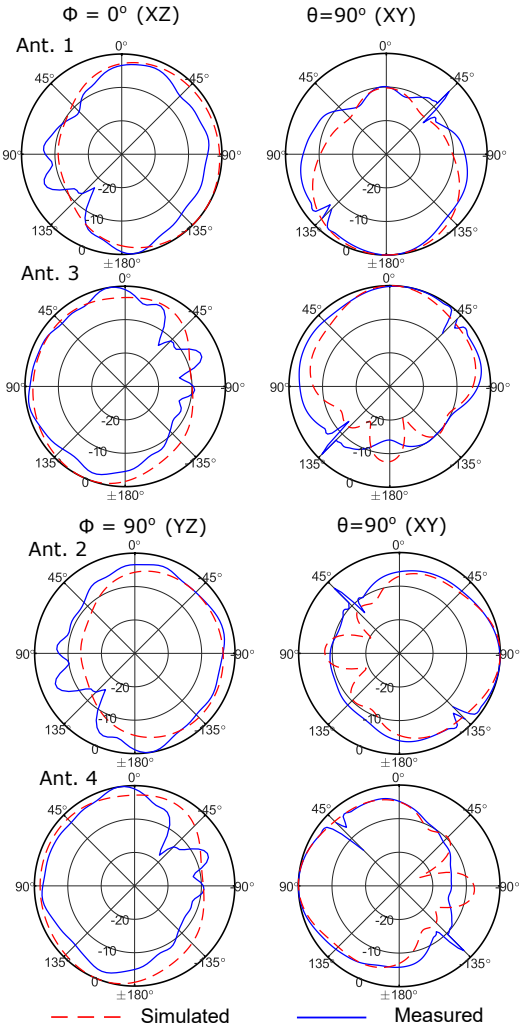

FIGURE 11. Normalized 2D radiation patterns for Ant. 1 to Ant. 4 at 3 GHz.

TABLE 1. Peak realized gain (dBi) at sub-6 GHz and mm-wave bands.

Frequency (GHz)	2.7	3.0	3.4	27	28	29
Simulated	3.7	4.6	4.4	9.4	9.4	8.7
Measured	3.6	3.9	4.5	9.1	9.8	9.8

Finally, the radiation patterns in xy-plane ($\theta = 90°$) verify that the whole antenna system provides spatial coverage of 360°. This can also be observed from Fig. 15, showing the total scan pattern at $\theta = 90°$ for $f = 28$ GHz. The total scan pattern is obtained as the maximum of the realized gain from all antenna elements. The results in Fig. 15 demonstrate capability of the MIMO antenna system in achieving 360° beam coverage in the azimuth plane. The simulated and measured gain variation in the total scan pattern is about 3.3 dB.

This article has been accepted for publication in a future issue of this journal, but has not been fully edited. Content may change prior to final publication. Citation information: DOI 10.1109/ACCESS.2022.3172931, IEEE Access

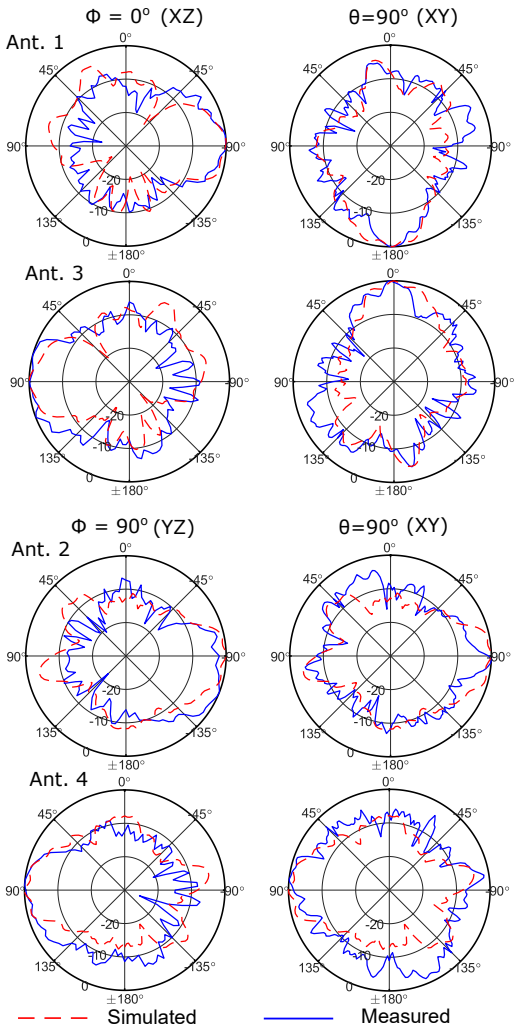

FIGURE 12. Normalized 2D radiation patterns for Ant. 1 to Ant. 4 at 28 GHz.

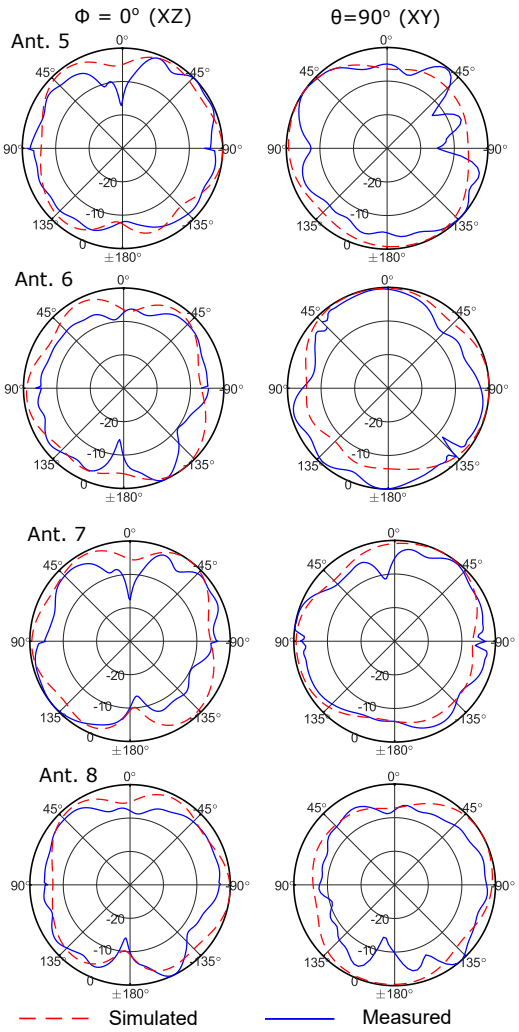

FIGURE 13. Normalized 2D radiation patterns for Ant. 5 to Ant. 8 at 3 GHz.

IV. CONCLUSION

A compact shared-aperture multi-beam and multi-band MIMO antenna system has been presented for 5G Vehicle-to-Everything (5G-V2X) application. The fundamental radiating component of the proposed MIMO antenna system is the hybrid tapered slot - dipole antenna which can operate at both microwave and mm-wave bands. Specifically, the design covers 2.45 GHz, 2.6 GHz, and 3.4 GHz (WLAN, LTE, 5G) sub-6 GHz bands and 28 GHz (5G) mm-wave band. Moreover, the antenna achieves a gain of more than 9 dBi at the mm-wave range and 4 dBi at the microwave range. The proposed MIMO antenna has demonstrated the capability to provide full coverage in azimuth plane which is especially useful for 5G-V2X communication.

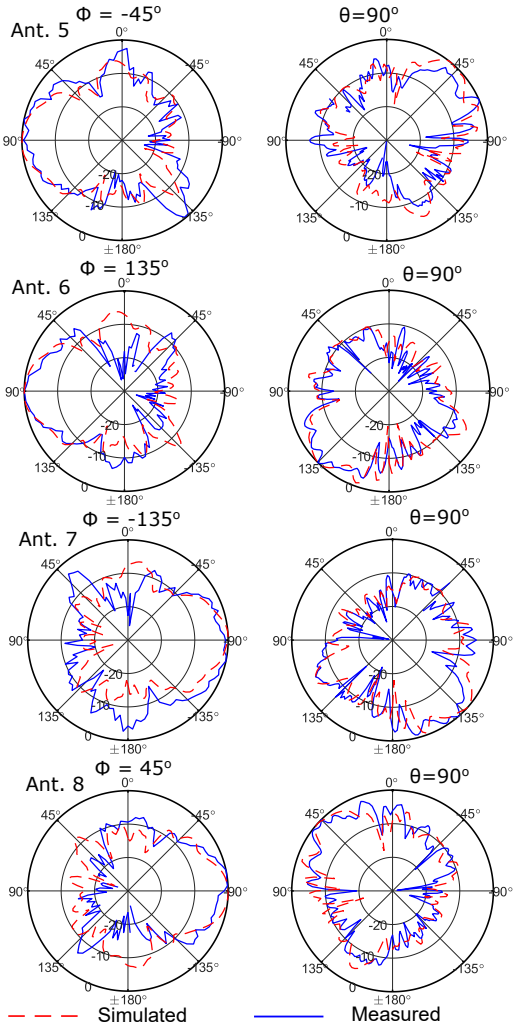

FIGURE 14. Normalized 2D radiation patterns for Ant. 5 to Ant. 8 at 28 GHz.

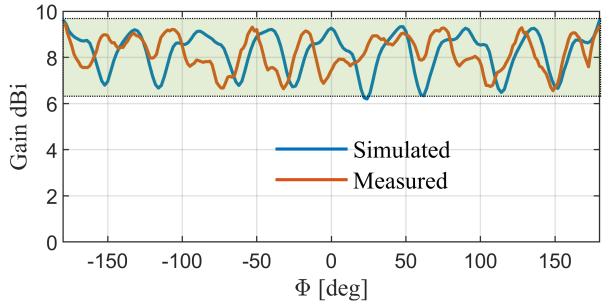

FIGURE 15. Total scan pattern in azimuth plane, i.e. maximum realized gain across all antennas at $\theta = 90^\circ$ at 28 GHz.

REFERENCES

[1] M. Eisenbarth, M. Wegener, R. Scheer, J. Andert, D. S. Buse, F. Klingler, C. Sommer, F. Dressler, P. Reinold, and R. Gries, "Toward smart vehicle-to-everything-connected powertrains: Driving real component test benches in a fully interactive virtual smart city," IEEE Vehicular Technology Magazine, vol. 16, no. 1, pp. 75–82, 2021.

[2] M. N. Sial, Y. Deng, J. Ahmed, A. Nallanathan, and M. Dohler, "Stochastic geometry modeling of cellular v2x communication over shared channels," IEEE Transactions on Vehicular Technology, vol. 68, no. 12, pp. 11873–11887, 2019.

[3] R. Lu, L. Zhang, J. Ni, and Y. Fang, "5G Vehicle-to-Everything Services: Gearing Up for Security and Privacy," Proceedings of the IEEE, vol. 108, no. 2, pp. 373–389, 2020.

[4] B. Feng, J. Chen, S. Yin, C.-Y.-D. Sim, and Z. Zhao, "A Tri-Polarized Antenna With Diverse Radiation Characteristics for 5G and V2X Communications," IEEE Transactions on Vehicular Technology, vol. 69, no. 9, pp. 10115–10126, 2020.

[5] A. K. Arya, S. Kim, K. Ko, and S. Kim, "Antenna for IOT-Based Future Advanced (5G) Railway Communication with End-fire Radiation," IEEE Internet of Things Journal, pp. 1–1, 2021.

[6] M. Ikram, K. Sultan, M. F. Lateef, and A. S. Alqadami, "A Road towards 6G CommunicationâĂŤA Review of 5G Antennas, Arrays, and Wearable Devices," Electronics, vol. 11, no. 1, p. 169, 2022.

[7] K. m. Faizi, G. Moradi, R. S. Shirazi, S. Zhang, and G. F. Pedersen, "Wideband Vertically Polarized Antenna with Endfire Radiation for 5G Mobile Phone Applications," IEEE Antennas and Wireless Propagation Letters, pp. 1–1, 2020.

[8] C. Di Paola, S. Zhang, K. Zhao, Z. Ying, T. Bolin, and G. F. Pedersen, "Wideband Beam-Switchable 28 GHz Quasi-Yagi Array for Mobile Devices," IEEE Transactions on Antennas and Propagation, vol. 67, no. 11, pp. 6870–6882, 2019.

[9] J. Park, H. Seong, Y. N. Whang, and W. Hong, "Energy-Efficient 5G Phased Arrays Incorporating Vertically Polarized Endfire Planar Folded Slot Antenna for mmWave Mobile Terminals," IEEE Transactions on Antennas and Propagation, vol. 68, no. 1, pp. 230–241, 2020.

[10] S. Zhang, X. Chen, I. Syrytsin, and G. F. Pedersen, "A Planar Switchable 3-D-Coverage Phased Array Antenna and Its User Effects for 28-GHz Mobile Terminal Applications," IEEE Transactions on Antennas and Propagation, vol. 65, pp. 6413–6421, Dec 2017.

[11] R. K. Singh, A. Basu, and S. K. Koul, "A Novel Reconfigurable Microstrip Patch Antenna With Polarization Agility in Two Switchable Frequency Bands," IEEE Transactions on Antennas and Propagation, vol. 66, no. 10, pp. 5608–5613, 2018.

[12] J. Zhang, S. Zhang, Z. Ying, A. S. Morris, and G. F. Pedersen, "Radiation-Pattern Reconfigurable Phased Array With p-i-n Diodes Controlled for 5G Mobile Terminals," IEEE Transactions on Microwave Theory and Techniques, vol. 68, no. 3, pp. 1103–1117, 2020.

[13] E. V. P. Anjos, D. Schreurs, G. A. E. Vandenbosch, and M. Geurts, "Variable-Phase All-Pass Network Synthesis and Its Application to a 14-54 GHz Multiband Continuous-Tune Phase Shifter in Silicon," IEEE Transactions on Microwave Theory and Techniques, pp. 1–1, 2020.

[14] J. Helander, K. Zhao, Z. Ying, and D. SjÃűberg, "Performance Analysis of Millimeter-Wave Phased Array Antennas in Cellular Handsets," IEEE Antennas and Wireless Propagation Letters, vol. 15, pp. 504–507, 2016.

[15] N. Ojaroudiparchin, M. Shen, S. Zhang, and G. F. Pedersen, "A Switchable 3-D-Coverage-Phased Array Antenna Package for 5G Mobile Terminals," IEEE Antennas and Wireless Propagation Letters, vol. 15, pp. 1747–1750, 2016.

[16] I. Syrytsin, S. Zhang, and G. F. Pedersen, "User Impact on Phased and Switch Diversity Arrays in 5G Mobile Terminals," IEEE Access, vol. 6, pp. 1616–1623, 2018.

[17] Y. J. Cheng, W. Hong, and K. Wu, "Design of a substrate integrated waveguide modified R-KR lens for millimetre-wave application," IET Microwaves, Antennas and Propagation, vol. 4, no. 4, pp. 484–491, 2010.

[18] J. Lian, Y. Ban, Z. Chen, B. Fu, and C. Xiao, "SIW Folded Cassegrain Lens for Millimeter-Wave Multibeam Application," IEEE Antennas and Wireless Propagation Letters, vol. 17, no. 4, pp. 583–586, 2018.

[19] J. Lian, Y. Ban, J. Zhu, K. Kang, and Z. Nie, "Compact 2-D Scanning Multibeam Array Utilizing the SIW Three-Way Couplers at 28 GHz," IEEE Antennas and Wireless Propagation Letters, vol. 17, no. 10, pp. 1915–1919, 2018.

[20] J.-W. Lian, Y.-L. Ban, C. Xiao, and Z.-F. Yu, "Compact substrate-integrated 4 ÃŮ 8 butler matrix with sidelobe suppression for millimeter-wave multibeam application," IEEE Antennas and Wireless Propagation Letters, vol. 17, no. 5, pp. 928–932, 2018.

[21] R.-S. Chen, L. Zhu, S.-W. Wong, X.-Z. Yu, Y. Li, L. Zhang, and Y. He, "Low-Sidelobe Cavity-Backed Slot Antenna Array With Simplified Feeding Structure for Vehicular Communications," IEEE Transactions on Vehicular Technology, vol. 70, no. 4, pp. 3652–3660, 2021.

[22] N. Nie and Z.-H. Tu, "Dual-Band Antenna with Wideband Harmonic Suppression Based on Dual-Function Slot Structure," IEEE Antennas and Wireless Propagation Letters, pp. 1–1, 2021.

[23] R. Rodriguez-Cano, S. Zhang, K. Zhao, and G. F. Pedersen, "mm-Wave Beam-Steerable Endfire Array Embedded in a Slotted Metal-Frame LTE Antenna," IEEE Transactions on Antennas and Propagation, vol. 68, no. 5, pp. 3685–3694, 2020.

[24] M. Ikram, N. Nguyen-Trong, and A. M. Abbosh, "Realization of a Tapered Slot Array as Both Decoupling and Radiating Structure for 4G/5G Wireless Devices," IEEE Access, vol. 7, pp. 159112–159118, 2019.

[25] M. Zada, I. A. Shah, and H. Yoo, "Integration of Sub-6-GHz and mm-Wave Bands With a Large Frequency Ratio for Future 5G MIMO Applications," IEEE Access, vol. 9, pp. 11241–11251, 2021.

[26] M. Ikram, N. Nguyen-Trong, and A. M. Abbosh, "Common-Aperture Sub-6 GHz and Millimeter-Wave 5G Antenna System," IEEE Access, vol. 8, pp. 199415–199423, 2020.

[27] M. M. Samadi Taheri, A. Abdipour, S. Zhang, and G. F. Pedersen, "Integrated Millimeter-Wave Wideband End-Fire 5G Beam Steerable Array and Low-Frequency 4G LTE Antenna in Mobile Terminals," IEEE Transactions on Vehicular Technology, vol. 68, pp. 4042–4046, April 2019.

[28] K. Sultan, M. Ikram, and N. Nguyen-Trong, "A Multi-band Multi-beam Antenna for Sub-6 GHz and Mm-Wave 5G Applications," accepted in IEEE Antennas and Wireless Propagation Letters, pp. 1–1, 2022.

[29] D. Yang, S. Liu, and D. Geng, "A Miniaturized Ultra-Wideband Vivaldi Antenna With Low Cross Polarization," IEEE Access, vol. 5, pp. 23352–23357, 2017.

[30] M. Ikram, N. Nguyen-Trong, and A. Abbosh, "Multiband MIMO Microwave and Millimeter Antenna System Employing Dual-Function Tapered Slot Structure," IEEE Transactions on Antennas and Propagation, vol. 67, no. 8, pp. 5705–5710, 2019.

[31] K. Ebnabbasi, D. Busuioc, R. Birken, and M. Wang, "Taper Design of Vivaldi and Co-Planar Tapered Slot Antenna (TSA) by Chebyshev Transformer," IEEE Transactions on Antennas and Propagation, vol. 60, no. 5, pp. 2252–2259, 2012.

[32] M. Ikram, "Multi-Functional Antenna Structures for 4G/5G Wireless Communication Devices," 2021.

[33] W. Wang, Z. Zhao, Q. Sun, X. Liao, Z. Fang, K. Y. See, and Y. Zheng, "Compact quad-element vertically-polarized high-isolation wideband mimo antenna for vehicular base station," IEEE Transactions on Vehicular Technology, vol. 69, no. 9, pp. 10000–10008, 2020.